Prediction of the sound transmission through a simplified front end model of a car.

Maria Gavila Lloret, Gregor Müller, Fabian Duvigneau, Ulrich Gabbert

Abstract

The introduction of stricter exhaust emission standards for passenger cars intensifies the trends towards more efficient vehicles. This can be achieved, for example, by using smaller engines, increasing the combustion pressure, or reducing the total weight of the vehicle. Furthermore, comfort expectations of the customers increase, whereas regulations on noise limits become more demanding. All these factors together represent a major challenge for the development process, in which the comfort requirements are constantly in conflict with the costs, the weight and the space limitations. Reaching the best compromise requires a consistent concept that simultaneously considers the characteristic of the engine sound radiation, the distribution of the noise control treatments in the vehicle, and the acoustic properties of the passenger cabin. Such an optimization is possible during the early virtual stages of the development process, provided that appropriate models are available for the different parts of the transmission chain.

In this article, a simplified model of the vehicle's front end is investigated. This example is formed by a steel plate and a three-sided plastic cover, which represent the firewall and the dashboard of the vehicle, respectively. Together with two acoustically rigid side walls, a closed air cavity is built. First, the setup and the numerical model are introduced. Two different concepts for the noise reduction based on poroelastic materials are tested, namely the insulation through a spring-mass component and the absorption of a porous layer. The acoustic response of the system is calculated using different formulations for the description of the poroelastic layers, and the results are compared to measurements at a window test bench. Finally, recommendations on the modeling approaches and an outlook to more realistic models are presented.

Kurzfassung

Die Einführung von strengeren Abgasemissionsvorschriften für die Automobilindustrie verstärkt immer mehr den Trend hin zu effizienteren Fahrzeugen. Daraus resultierende Abhilfemaßnahmen sind beispielweise die Entwicklung von kleineren Motoren, die Erhöhung des Verbrennungsgasdruckes oder der Fahrzeugleichtbau. Darüber hinaus steigen die Erwartungen der Kunden an der Fahrkomfort, während die Schallemissionsvorschriften immer wieder strenger werden. Diese Faktoren stellen eine große Herausforderung für den Fahrzeugentwicklungsprozess dar, in dem die Komfortanforderungen stets mit den Kosten-, Gewichts- und Raumbegrenzungen im Widerspruch stehen. Um dabei den bestmöglichen Kompromiss zu erreichen, bedarf es der gleichzei-

tigen Betrachtung der Motorgeräuschabstrahlung, der Verteilung der Schallisolationsmaterialien im Fahrzeug und den akustischen Eigenschaften des Innenraumes. Eine derartige Optimierung ist während der virtuellen Projektphase effizient möglich, setzt aber die Verfügbarkeit von geeigneten Simulationsmodellen für die einzelnen Schallübertragungsschritte voraus.

In dieser Arbeit wird ein vereinfachtes Fahrzeugvorderwagenmodell untersucht. Das Beispiel besteht aus einer Stahlplatte, die die Stirnwand repräsentiert und einer dreiseitigen Kunststoffverschalung, die die Instrumententafel darstellen sollen. Zusammen mit den beiden schallharten Seitenwänden bilden diese Flächen ein geschlossenes Luftvolumen. Zuerst werden die Versuchsbedingungen und das numerische Modell vorgestellt. Zwei verschiedene, auf poroelastische Materialien basierende Konzepte werden untersucht: die Schalldämmung über ein Feder-Masse System und die Absorption durch ein poröses Material. Die transmittierte Schallleistung dieser Aufbauten wird auf Basis verschiedener Formulierungen für das poroelastische Material berechnet und zu Validierungszwecken mit Messergebnissen aus einem Fensterprüfstand verglichen. Abschließend werden aus den erzielten Ergebnissen Empfehlungen für die Modellbildung abgeleitet sowie ein Ausblick auf die Erstellung realitätsnäherer Modelle präsentiert.

1. Introduction

The automotive industry is undergoing a time full of changes and innovations: „In our view the next 10 years are probably going to involve more change and more dynamics than we have seen in the last 100“ are words of former BMW’s Sales and Marketing Chief, Ian Robertson, in 2016 [1]. The ongoing trends have a notable impact on the acoustic performance of vehicles, too. To name a few examples, the development of more efficient cars with reduced fuel consumption has led to engine downsizing, which generates a louder excitation level, and to the extension of lightweight design concepts that results in a decreased basis insulation of the car body. The expansion of hybrid and electric powertrains radically modifies the traditional sound characteristics of internal combustion engines as well as they unmask some noise sources that were before imperceptible for the driver and the passengers. Moreover, the numerous sensors and control devices required by the new driving assistance systems with perspective towards autonomous driving require additional construction space and numerous holes for power and data lines, which limit the available volume for acoustic treatments. However, the customers’ expectations of comfort and quality perception is constantly increasing, especially in the premium segment. Moreover, shortened development times and the reduction of prototype hardware intensify the need to have reliable prediction models.

In order to face this challenging objective to meet all the project specifications and to deliver a high quality product, it is necessary to consider all the requirements in the early design stages, so that optimized solutions could be found. With regard to the acoustic performance of the vehicles, this entails the availability of robust predictions in the first development phases, which are mostly virtual. Such design tools have to enable a comparison among different design concepts and should finally be able to relate the obtained results to the customer’s perception. Because of the high complexity of the propagation phenomena, it is preferable to make use of a hybrid approach,

the combination of experiments and computer-aided simulations to achieve accurate results. In the following Section 2, we introduce the hybrid methodology on the basis of the sound transmission through the vehicle front. In Section 3 we present the simplified front end model on which the investigations are conducted, and in Section 4 we focus on the numerical modeling of different concepts for noise control treatments (NCT). Finally, the main conclusions are summarized in Section 5, where also an outlook to future developments is given.

2. Hybrid approach for sound transmission prediction

The description of the sound propagation around and inside a vehicle is highly complicated due to the various parallel transmission paths and the interactions among components at both local and global levels (e.g. modal response of the inner air cavity and the car body). In order to address this problem, we divide the transmission chain into its three substantial components, namely the noise source, the main structural components and the observation point, as depicted in Figure 1. The link between the components is included by means of several input and output transfer functions (TF_i, TF_o).

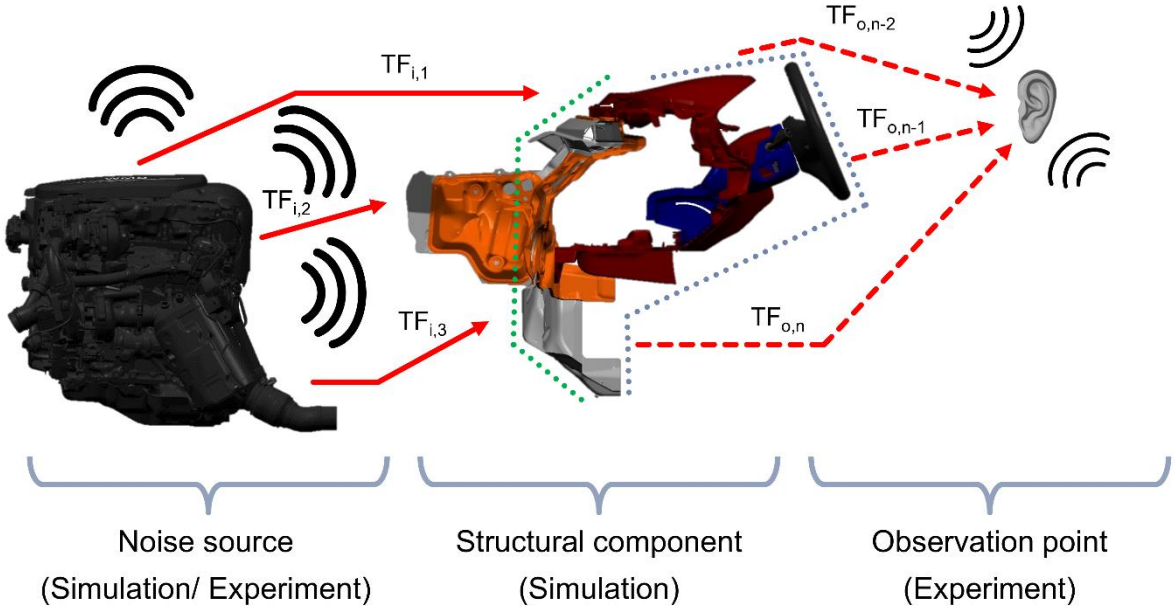

Figure 1. *Hybrid method for sound transmission prediction applied to the front car end.*

Within the current research, we focus on the implementation of a hybrid approach to predict the airborne sound transmission through the front car end. In this case, the engine is one of the most important noise sources. The operation of the powertrain and its aggregates generates vibrations on their surfaces that are radiated into the surrounding air in form of pressure fluctuations. These waves propagate in the engine compartment and impinge on the firewall. The corresponding transfer functions that relate the excitation to the pressure and velocity distributions on the firewall surface (green dotted lines in Figure 1) can either be the result of a simulation [2] or be measured in an engine test bench. Any other noise source can be evaluated in the same way.

The next step of the transmission chain is formed by the structural components. The input information derives from the acoustic power distribution generated by the excitation. The propagation of energy through the system is calculated with help of a numerical model. In the next section we provide a detailed description of an exemplary simulation setup. The results of the calculation are the pressure and the normal velocity obtained on the contact surface between the structure and the next component. These two quantities define the radiated power that is transmitted inside the passenger's cabin. For an accurate prediction of the transmission it is also necessary to account for the absorption and reflection properties of the passenger's cabin itself. To this end, and based on the technique employed in the panel contribution analysis [3], we make use of reciprocal measurements for the determination of the output transfer functions in the real environment. This means that a calibrated noise source is placed at the observation point (e.g. at the driver's ear) and the resulting acoustic pressure and velocity fields on the interface to the structural component are measured. Lastly, the inversion of the reciprocal transfer functions enables the projection of the output of the structural component on the observation point.

The introduced hybrid method allows for the characterization of each one of the three subsystems (see Figure 1) of the transmission chain separately from the other two components. This independence is an approximation of the real behavior since, especially at lower frequencies, global interactions may be present. The main advantage is that every component can be evaluated by the most adequate method, experimental or numerical, based on the information at disposal and the development stage. Examples of this are data obtained from a predecessor model or results from simplified geometries at the early design phases. The detail level of the components is updated in the course of the development process as soon as new and more accurate data are available. The detailed representation of the excitation distribution on the firewall as well as on the measured inner cavity transfer functions allow to obtain accurate acoustic predictions taking into consideration the real operational conditions and the environment of the structural component.

3. Simplified front car end for airborne sound transmission

In this section, we draw attention to the description of the structural component of the sound transmission chain. A proof-of-principle model serves here as object of the investigations, in which the substantial components of the front section of the vehicle are present. This mock-up has a hexahedral shape with the dimensions 0.85 m x 0.4 m x 0.5 m (see Figure 2). The two smaller lateral walls are structurally and acoustically rigid and represent the side walls of the car. They build the support on which a three-faced cover made of a thermoplastic Plexiglas® is fixed. The material for these surfaces is 1.5 mm thick and has been selected to match the properties of the vehicle's dashboard in terms of mass density per unit area. On the remaining large surface there is an opening of size 0.85 m x 0.43 m in which we represent the firewall with a 0.75 mm thick steel plate, a common thickness in the vehicle construction. All six faces together enclose an air cavity.

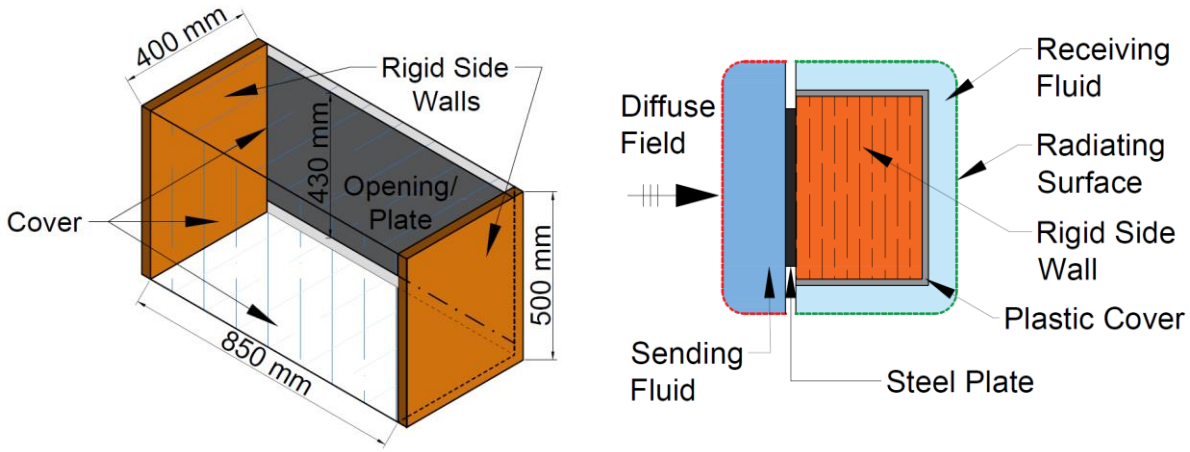

Figure 2. *Schematic representation of the simplified front car end model: isometric view with dimensions (left); side view including sending and receiving fluids (right).*

During the experimental and numerical analyses, a pressure diffuse field is the excitation that acts on the system, either directly on the opening surface of the cavity or on the steel plate, depending on the configuration setup. The acoustic energy propagates inside the air cavity and induces vibrations in the plastic cover, which lastly radiates into a semi-free field environment.

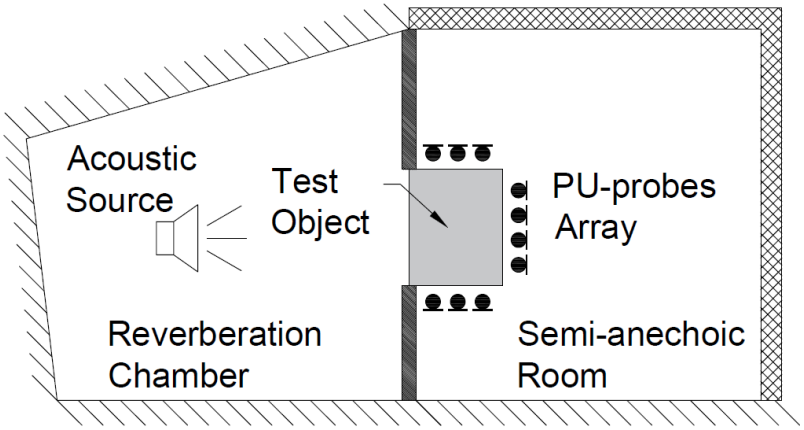

Figure 3. *Schematic representation of the window test bench.*

A reference data set is obtained from the experimental investigations. To this end, the mock-up is measured in a window test bench; its basis elements are displayed in Figure 3. The incoming pressure field is produced by a loudspeaker located in the reverberation chamber, whose size ensures a diffuse pressure distribution above 80 Hz, whereas the semi-anechoic room guarantees the proper free wave propagation conditions in this frequency range. The partition wall separating the two rooms has an aperture in which the tested plastic cover is placed, as the photos in Figure 4 show. The opening surface of the cavity coincides with the plane of the wall, while the plastic cover is situated in the semi-anechoic room. With help of an array of PU-probes the external surface area of the cover is scanned so that the pressure and the normal velocity at 400 points are available. This information is employed to calculate the total radiated power of the structure as:

$$W_{rad} = \sum_{i=1}^{N} p_i \cdot v_{n,i} \cdot S_i \qquad (1)$$

where S_i is the scanned surface corresponding to each of the N = 400 probe positions. The PU-probes were calibrated for measurements up to 4 kHz. However, for some highly insulating configurations, the radiated energy of the structure is so low above a certain frequency value that the background noise dominates the measured power and no reliable information is obtained. Such cases are later indicated.

The finite element model for the numerical investigations includes all the subsystems introduced in the experimental setup. The steel plate and the plastic cover are modeled with solid shell elements, special elements that help to alleviate the locking issues in very thin structures. The nodes of a solid shell element have three degrees of freedom (DOF), one for each displacement component. On the outer edges of the structural parts the displacements of the nodes are restricted in the direction of the thickness to represent the simply supported boundary conditions of the test bench. Inside the structure, the enclosed air cavity is discretized with hexahedral elements, which have a single pressure DOF per node. The four large faces of the fluid cavity are directly coupled to the plate and the plastic cover to enable the energy transmission, while on the two rigid side walls a zero normal velocity is imposed to ensure the perfect reflection of the acoustic wave.

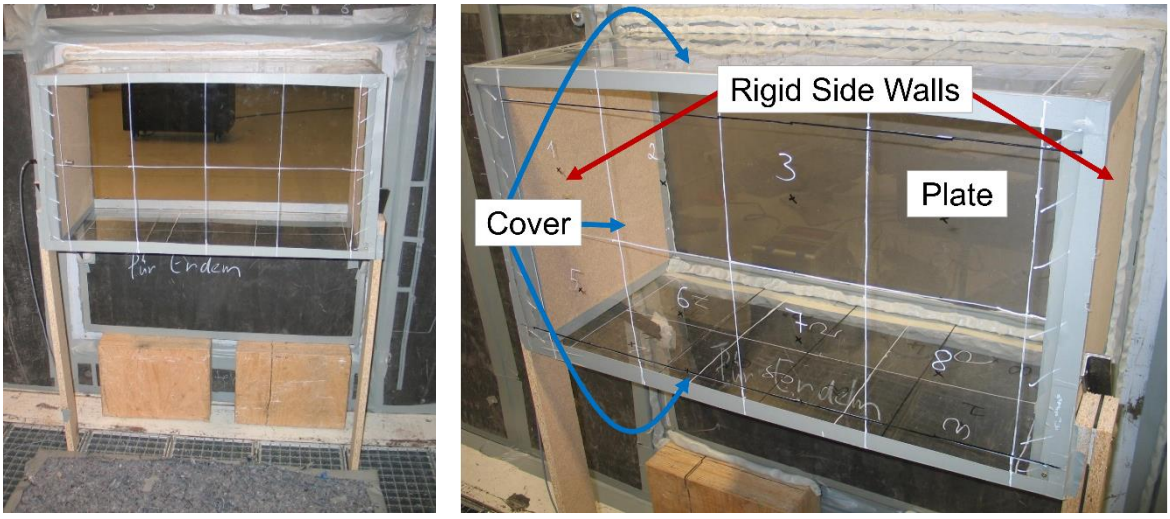

Figure 4. *Two views of the simplified front car end installed in the window test bench for the experimental investigations: open cavity (left), closed cavity (right).*

The reverberation and semi-anechoic rooms are modeled by a combination of finite fluid volume elements with infinite elements applied on their outer layer. This is a standard procedure to numerically extend a fluid domain and to guarantee free wave propagation. As displayed in Figure 2 (right), the diffuse field excitation is applied on the outer surface of the sending fluid (marked in red) and the total radiated power is calculated through the external surface of the receiving fluid (colored in green). The size of the sending and receiving finite volumes has been selected large enough so that actually free wave propagation is ensured and the results are not influenced by the finiteness of the volumes. The lowest frequency considered in the numerical investigations is 80 Hz, value above which the diffuse field condition is guaranteed in the experimental reverberation chamber. The upper frequency limit is 2 kHz, so that the range in which the airborne engine radiation through the front car end dominates the sound level in the passenger's cabin is counted in.

3.1 Comparability between experimental and numerical setups

Before studying the performance of different noise control treatments, some tests were conducted to assess the equivalence between measured and simulated results. For this purpose, we have compared the behavior of the system when the cavity is open to the excitation fluid, i.e. if the steel plate is removed, and when the steel plate is used to complete the enclosure. For the numerical modeling of the open configuration the steel plate component has been deleted. An interface component is applied to link the fluids of the sending volume and of the inner cavity. This is a numerical tool that projects the pressure information between the two surfaces that are usually in contact with the steel plate, so that the void left by the plate is bypassed and the total fluid volume remains unchanged. The results of all simulated and measured configurations are presented in terms of the insertion loss (IL, equation (2)). In this section it is defined as the difference of the radiated power of the plastic cover to the sending fluid when the cavity is open and when the cavity is closed by the steel plate.

$$IL\ [dB] = W_{rad}^{open}[dB] - W_{rad}^{plate}[dB] \tag{2}$$

As part of the model construction, different influence factors affecting the comparability between the experimental and virtual results were investigated in detail. To that end, we have made use of the basis plastic cover geometry in open and closed configurations, that is, only fluid and structural components have been considered at this stage. Among the analyzed parameters we have highlighted the boundary conditions of the structural components and the fluid damping inside the air cavity. This damping is introduced as the imaginary part of the sound speed, as indicated in [4].

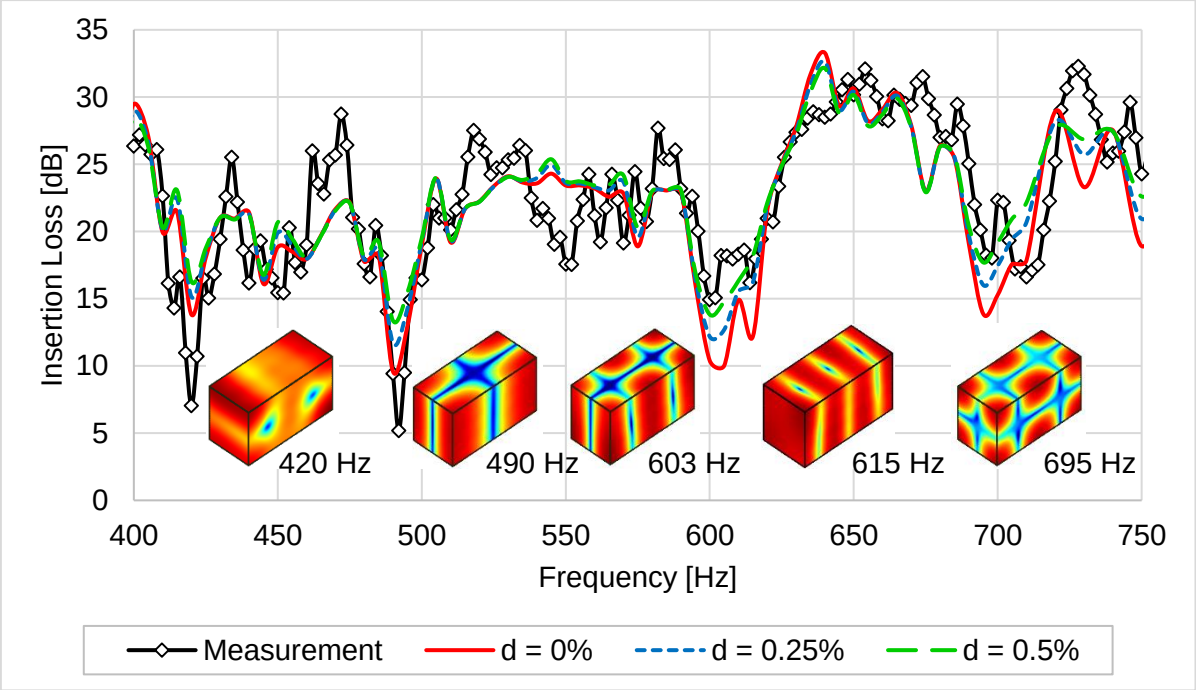

Figure 5. *Insertion loss results from measurement and simulations for the air cavity closed by the steel plate. Different damping values for the inside fluid are compared. Narrow band results.*

In our study we have observed that the boundary conditions of the steel plate and of the plastic cover only slightly modify the results at the frequency range under 100 Hz. On the contrary, the fluid damping inside the air cavity has been identified as the parameter with the largest impact on the mid and high frequency results. In Figure 5, we

compare the response of the experiment and the simulations with different fluid damping values, namely 0%, 0.25% and 0.5% in the frequency range between 400 Hz and 750 Hz. The overall correspondence with the measured insertion loss curve is good, with some exceptions at the total minima and maxima levels. Next, we focus on the numerical prediction of the cavity resonances, whose mode shapes have been included next to each peak in the diagram. These resonances are especially strong for the closed configuration if resonance phenomena occur in the cavity. This is the reason why the influence of the fluid damping is only noticeable at the resonances of the cavity. For the peaks at approximately 420 Hz and 490 Hz the undamped system gives the best correspondence to the measured results. But for the (2 1 0) and (3 0 0) cavity eigenmodes at 603 Hz and at 615 Hz the best match is obtained with a damping value of 0.5%. At the 695 Hz resonance a 0.25% fluid damping yields the closest approximation to the experimental data.

The high frequency response is analyzed in Figure 6, which also compares the experimental and the numerical results. Since above a certain frequency value the modal density increases and the overlap of eigenmodes makes the distinction of single resonance peaks no longer possible, we prefer to average all following results in third octave bands to improve legibility. The calculations show that the numerical model with a reduced damping coefficient of 0.25% matches best with the measured data in the high frequency range.

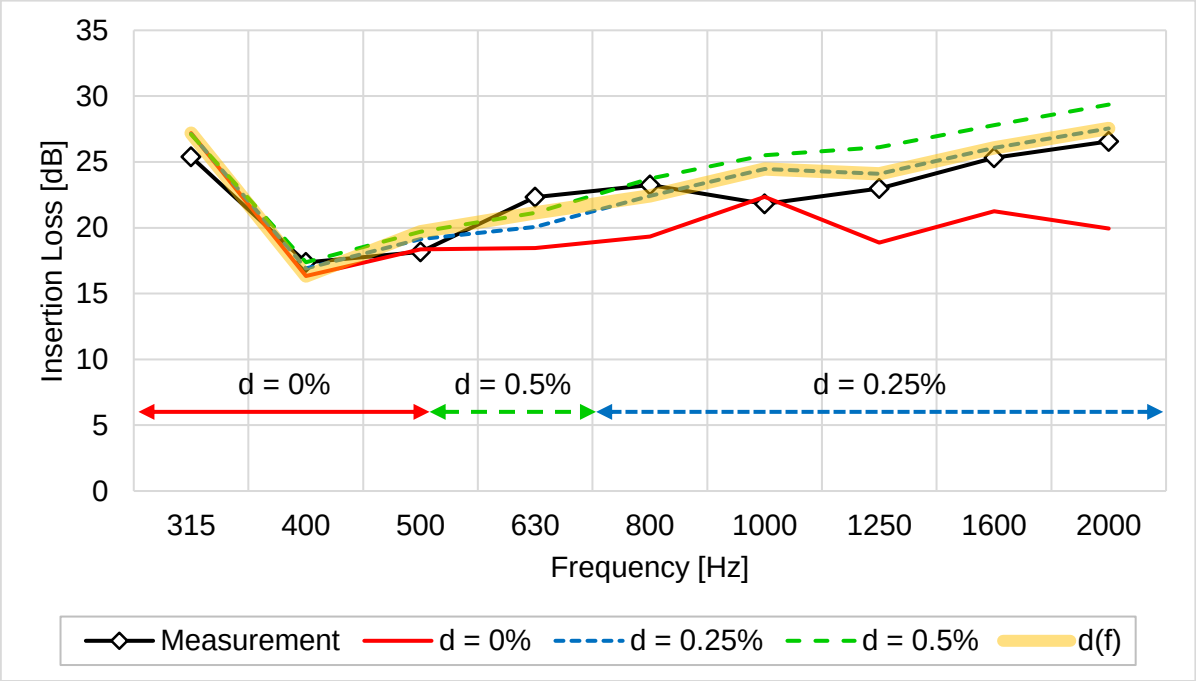

Figure 6. *Insertion loss results from measurement and simulations for the air cavity closed by the steel plate. Different damping values for the inside fluid are compared. Results are averaged in third octave bands.*

From the mid- and high frequency responses calculated in this section we derive a fluid damping profile for the cavity that is employed in the following investigations: undamped inner fluid up to 500 Hz, a damping coefficient of 0.5% between 500 Hz and 690 Hz (just before the (2 1 1) cavity eigenmode), and 0.25% damping above this frequency. The resulting IL curve with frequency dependent damping profile *d(f)* is indicated in Figure 6 by an orange shading.

4. Modeling different concepts for noise control treatments

A key factor towards reliable acoustic airborne predictions is the accurate representation of the noise control treatments. Typical examples of passive acoustic treatments in the automotive industry include absorbers, spring-mass systems, and the combination of both in three-layered systems. All three concepts have one common element: the presence of one or more poroelastic components. Poroelastic media are biphasic materials formed by a solid elastic frame, also called skeleton, whose pores are filled with a fluid, usually air. Due to their biphasic nature and the resulting interactions between the two constitutive phases, the modeling of poroelastic media presents an additional challenge in comparison to traditional elastic or fluid materials: energy dissipation does not only arise from elastic damping losses or fluid dissipation, but the coupling between the two phases must be considered too.

Within the scope of the current investigation, we have tested different material models based on the poroelasticity theory by Biot-Allard [5], [6] and compare their performance. This theory avoids the resolution of the individual pores at the microscale and treats the material as a homogenized medium in which the two phases are simultaneously present. The equations (3) and (4) govern the dynamic behavior of the material for harmonic time dependence $e^{j\omega t}$ as:

$$\nabla \underline{\underline{\hat{\sigma}}}^{s}\left(\underline{u}\right) + \omega^2 \cdot \tilde{\rho} \cdot \underline{u} + \tilde{\gamma} \cdot \nabla p = 0 \tag{3}$$

$$\Delta p + \frac{\tilde{\rho}_{22}}{\tilde{R}} \cdot \omega^2 \cdot p + \frac{\tilde{\rho}_{22}}{\phi^2} \cdot \tilde{\gamma} \cdot \omega^2 \cdot \nabla \underline{u} = 0 \tag{4}$$

where j denotes the imaginary unit $\sqrt{-1}$ and ω is the pulse frequency. The acoustic pressure p and the solid phase displacement $\underline{u}$ are the state variables of a poroelastic compound. The stress tensor $\underline{\underline{\hat{\sigma}^s}}$ is exclusively a function of the solid phase assumed in vacuo. The tilde symbol indicates that the corresponding quantity is complex and frequency dependent. The total effective dynamic density $\tilde{\rho}$ and the mass coefficient of the fluid phase $\tilde{\rho}_{22}$ account for the inertial and viscous couplings, whereas the coefficient $\tilde{\gamma}$ contains the potential coupling. The elastic coefficient $\tilde{R}$ is the bulk modulus of the air occupying a fraction ϕ of the volume, where ϕ indicates the open porosity, i.e. the fraction of fluid phase volume with respect to the total aggregate volume. Appropriate expressions for the complex coefficients are given, for example, by the semi-phenomenological model proposed by Johnson-Champoux-Allard (JCA) [7], [8]. These relations link the aforementioned dynamic quantities to the parameters describing the microstructural properties of the poroelastic material: flow resistivity σ, viscous characteristic length Λ, thermal characteristic length Λ' and tortuosity α_∞. The determination of these properties is complex, requires special measurement equipment and not all the procedures are standardized.

The resolution of the equation system above is cumbersome and requires a large number of input parameters (for example, nine input parameters are needed for the JCA formulation). So, one may make use of simplified formulations in order to reduce the characterization effort and the computational cost. On the one hand, if the influence of the fluid phase can be neglected, the first two terms of equation (3) describe the dynamic behavior of the skeleton in vacuo. In this case, the material can be modeled as a classical elastic solid. Hence we later refer to this model as *elastic*. On the other hand, the first two terms in equation (4) represent the Helmholtz equation for the fluid

phase when the interaction of the frame with the air is neglected, either if the skeleton is assumed to be motionless, or if it has a minor contribution to the total stiffness. We identify this model as *porous*. The ranges of application of the one or the other formulation are, however, not clearly delimited and depend not only on the material properties themselves, but also on the coupling conditions of the poroelastic system to other components [9]. In all analysis displayed below the material model of the noise control treatment is the only variable factor with the aim to determine the most appropriate modeling for a given application.

4.1 One-layered system: Absorber

Next, we employ the cavity configuration introduced in Section 3 to analyze the behavior of several noise control treatment concepts and to assess the suitability of the three aforementioned material formulations. A single layer of poroelastic material, commonly called *absorber* because of its noise absorbing properties, is the first object of investigation. This 25 mm-thick layer is a relatively stiff foam (Young's modulus E = 0.11 GPa), has a low damping value (damping coefficient η = 0.08) and its surface is open-pored, meaning that the air can penetrate and go through the layer. For all following tested configurations the steel plate is present, so that a closed air cavity is built. The evaluation of the treatment's performance is, analogously to the former section, given in terms of the insertion loss. Although, for all the following results, the reference state is the cavity closed with the steel plate, as indicated in equation (5).

$$IL\,[dB] = W_{rad}^{plate}[dB] - W_{rad}^{NCT}[dB] \tag{5}$$

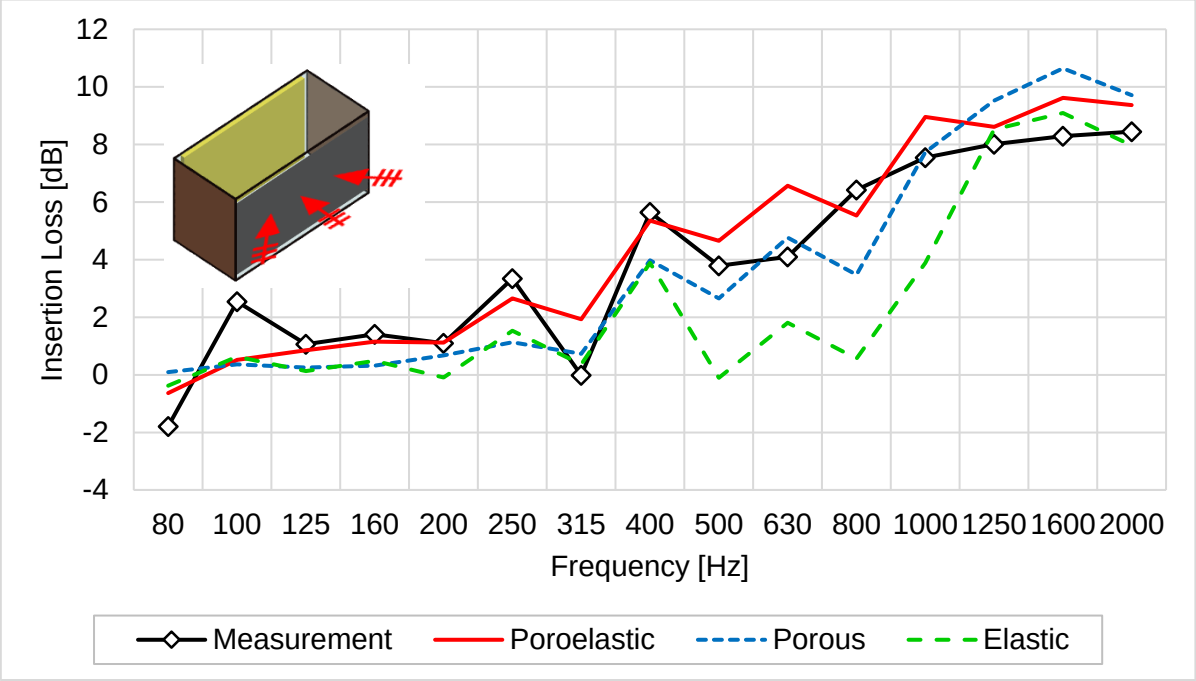

Figure 7. *Insertion loss results from measurement and simulations for a foam layer (yellow) placed on the inner front face of the plastic cover. Different material models for the foam layer are compared.*

Figures 7 and 9 display the insertion loss results for two different absorber positions. The total area covered by the absorber layer remains the same. First, for the state depicted in Figure 7, the foam is placed inside the cavity on the front face of the plastic cover. The frequency response of the poroelastic and the porous models show trends close to the measured data. The system with poroelastic formulation performs better in terms of the insertion loss. The differences between the results of these two models can be explained by the direct coupling of the noise control treatment to a vibrating component. This additional structural damping that the foam layer introduces in the plastic cover is only considered in the poroelastic model.

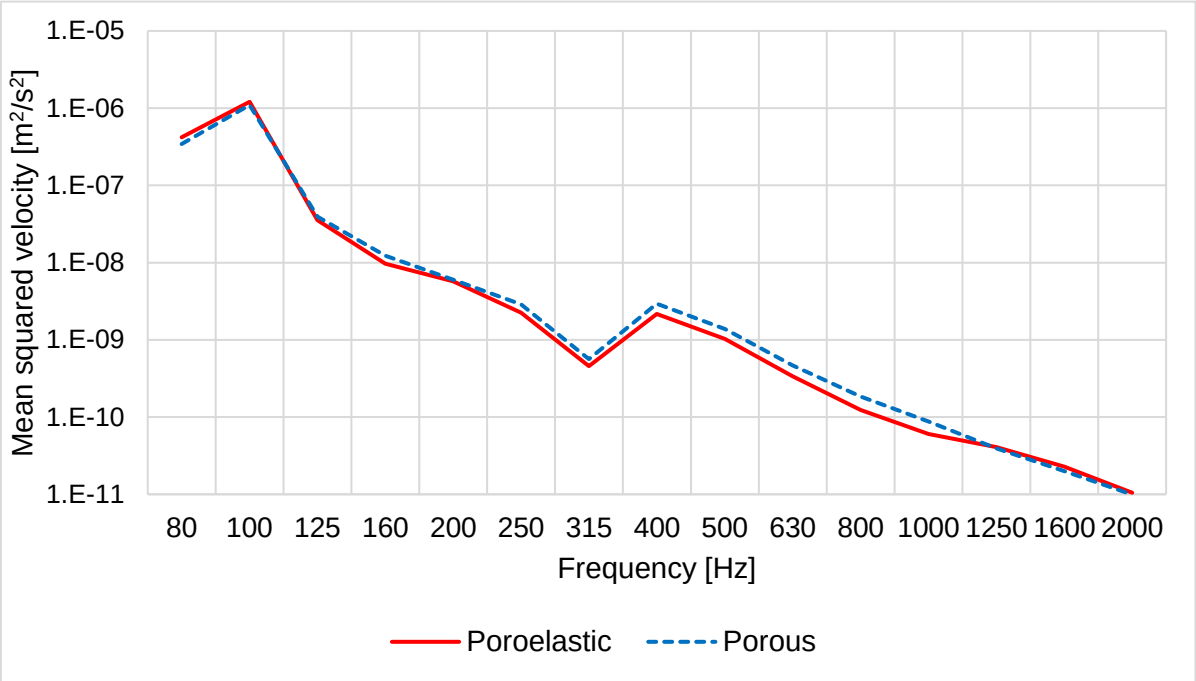

Figure 8. *Mean squared velocity on the plastic cover component for a foam layer placed on the inner front face of the cover. Comparison between poroelastic and porous model for the foam material.*

This effect can be observed in detail in Figure 8, where the mean squared velocity over the whole plastic component is shown. In the frequency range between 160 and 1250 Hz it can be noticed that the averaged velocity level on the cover is lower when the poroelastic model is applied since the foam's skeleton contributes to the damping. The need to include this additional structural damping in the model makes the poroelastic formulation the best suited for this application. The modeling as an elastic solid is missing the main dissipation factor, i.e. the energy losses by absorption. Consequently this model underestimates the total impact of the foam layer.

For the second configuration, the absorber is divided into two pieces of equal size, which are placed on the rigid side walls of the cavity. The coupling to a rigid backing reduces the displacement of the foam's solid frame significantly. This is the reason that the poroelastic and the porous formulations behave similarly above 200 Hz, as Figure 9 shows. In this situation, the use of the porous simplification can be recommended, because it results in a reduction of the number of degrees of freedom of the foam component from four DOFs in the poroelastic formulation (acoustic pressure and three displacement components) to just one DOF for the porous model (acoustic pressure). As a result, 20% computational time and 15% memory can be saved, which is a large decrease, since the foam component represents only 5% of the total number of nodes

in the model. Both, the poroelastic and the porous formulation are suitable for this configuration. The elastic simplification has a different curve progression than the measurement above 315 Hz because, as already mentioned, this model does not include the absorption effects that dominate in the mid and high frequencies.

We can state that, when modeling absorbing layers, the poroelastic model gives good results. Additionally, if the foam component is located on a rigid wall, the choice of the porous simplification supposes a reduction of computational resources without affecting the accuracy.

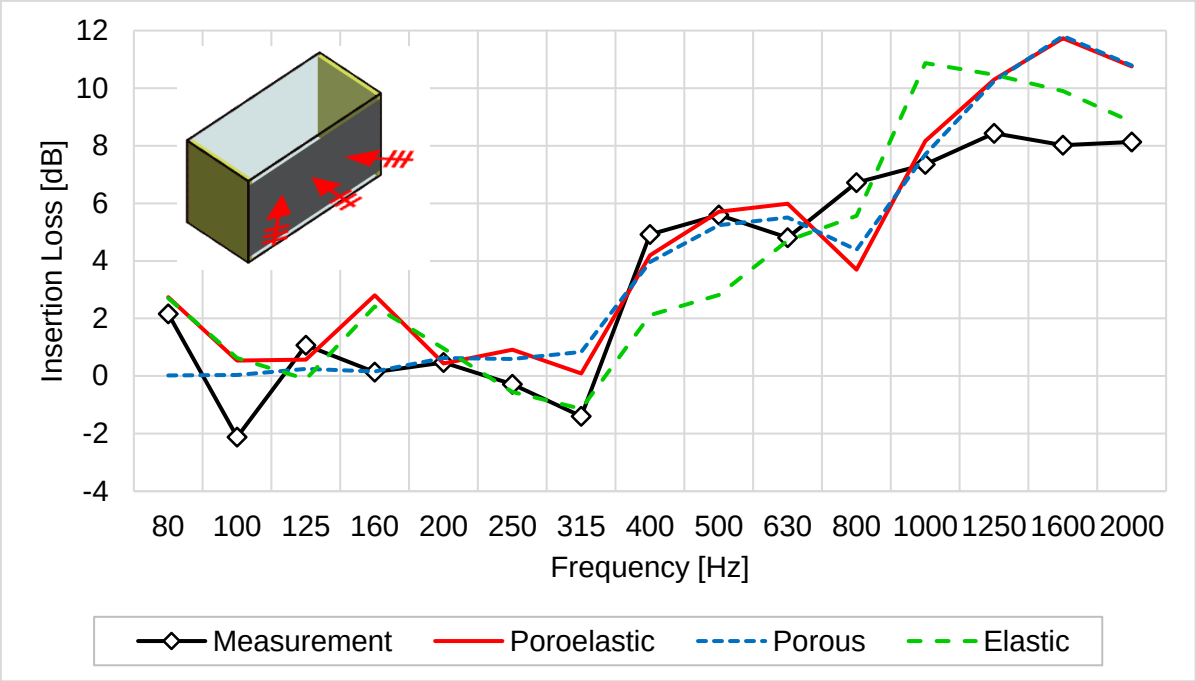

Figure 9. *Insertion loss results from measurement and simulations for two foam layers (yellow) placed on the rigid side walls of the cavity. Different material models for the foam layers are compared.*

4.2 Two-layered system: Spring-mass system

Displayed in Figure 10 (left) is the next analyzed noise control treatment: a spring-mass system that is attached to a vibrating structure. Such assemblies are composed of a metal sheet (vibrating structure), a foam layer (spring), and a thin heavy layer (mass). A spring-mass system possesses a promising insulation performance for frequencies above its spring-mass resonance. Therefore, it finds frequent application in the automotive industry. Due to the direct interaction with the steel plate and the heavy layer, i.e. with two structural components, the elastic properties of the middle layer gain significance in its dynamic behavior and determine the choice of an adequate material model. We have selected two foam materials with different elasticity characteristics in order to illustrate this fact.

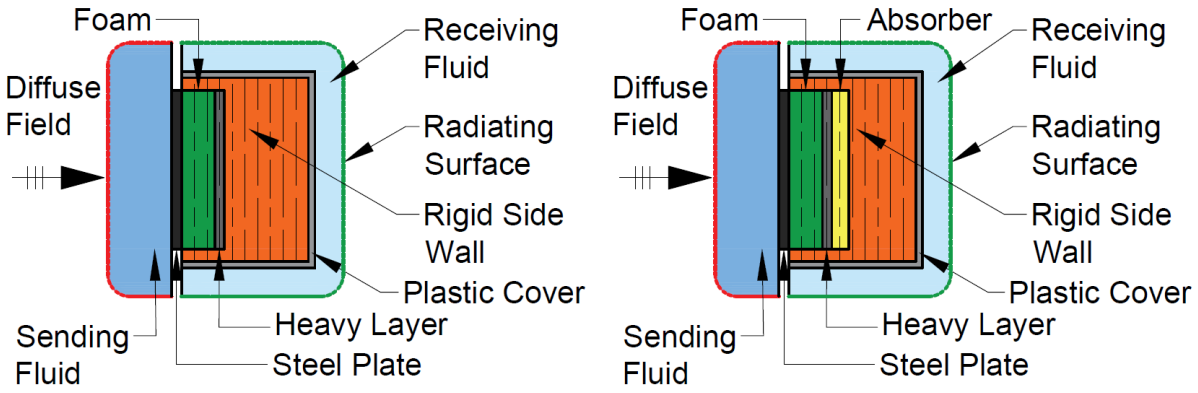

***Figure 10**. Schematic side view of the cavity models with NCT: (left) spring-mass system with spring foam colored in green; (right) the three-layered system with spring foam in green and absorber foam in yellow. The thicknesses of all components are not to scale. Refer to Figures 2 and 4 for clarity.*

First, we have studied the behavior of foam whose specific stiffness, that is the ratio between the Young's modulus E and the thickness d, is relatively low (E/d = 1 kPa/mm). The three available formulations for describing a poroelastic material were applied to the middle layer, while all other components in the model remain unchanged as elastic and fluid parts, respectively. In Figure 11 the insertion loss curves obtained from the numerical models are compared with the experimental data. We must point out that at 1600 Hz the radiated power reaches the minimum measurable level by the PU-probes over the background noise and, consequently, the obtained information for the two spring-mass systems are not reliable above this frequency and provide an IL value lower than the real one. This frequency range has been marked in Figure 11 and later also in Figure 12 with a dashed black-orange line.

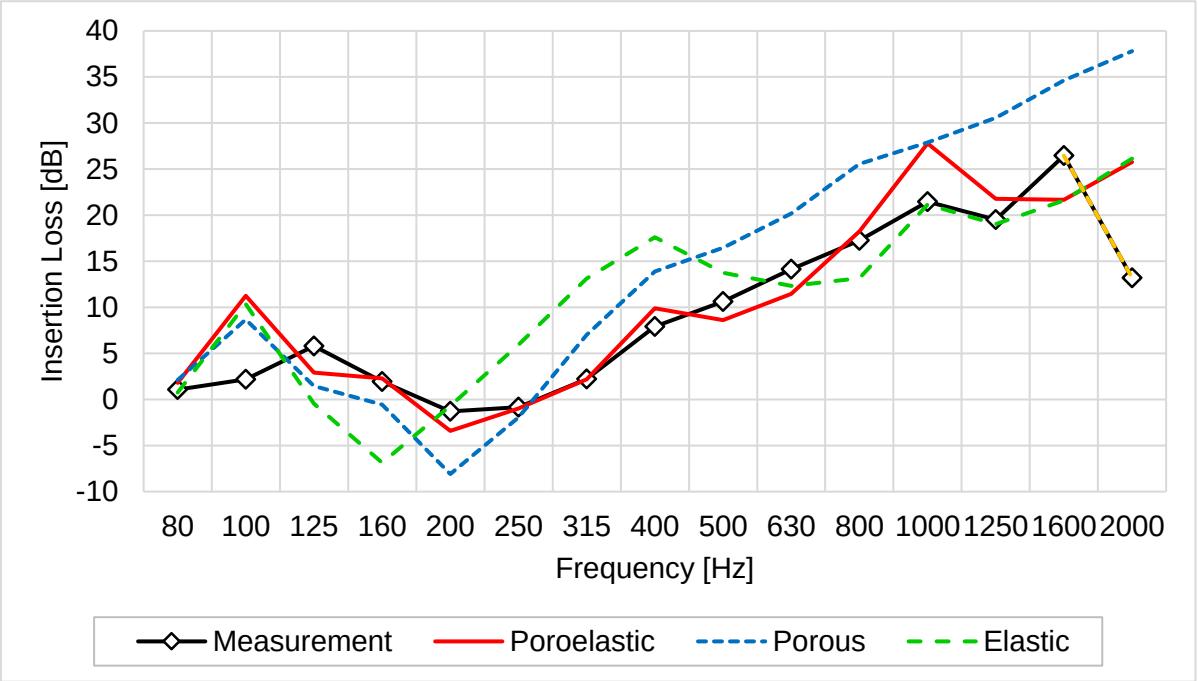

***Figure 11.** Insertion loss results from measurement and simulations for a spring-mass system. Different material models for the foam layer are compared.*

The two most important design criteria that should be correctly predicted by an accurate model of a spring-mass system are the spring-mass resonance and the high frequency slope of the insertion loss curve. For this relatively soft foam we observe that the poroelastic formulation fits the measured data best over the complete frequency range and gives an accurate prediction of the two aforementioned criteria. The porous model underestimates the performance at the spring-mass resonance (located at the 315 Hz third octave band) since the damping by the skeleton of the foam is not included, and it overestimates the high frequency behavior because the transmission of energy to the heavy layer is not as effective in the porous model as it is in reality. On the contrary, the absence of the fluid phase in the elastic simplification notably reduces the bulk stiffness of the aggregate, shifting the whole curve towards lower frequencies.

Second, we have investigated a foam with a higher specific stiffness (E/d = 4 kPa/mm). All other components, including the heavy layer, were the same as in the previous configuration. Figure 12 shows the measured IL values and the numerical results for the different material formulations. Opposed to the previous examples, the results of the elastic model come closest to the experimental data. Moreover, the overall trend is correctly captured. The curve progression obtained with the poroelastic description shows a good prediction of high frequency slope, but the insertion loss level is too low. This shift towards higher frequencies is indicative of an overestimation of the material's stiffness. The unsuitability of the porous model for this application has been explained above.

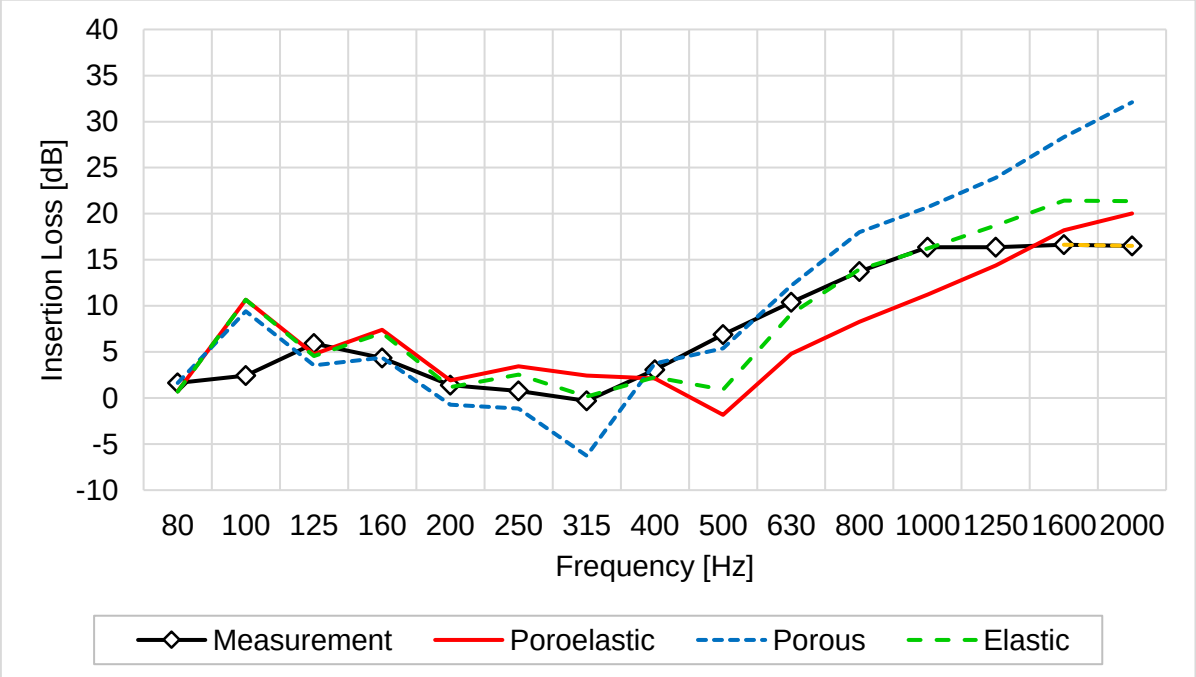

Figure 12. *Insertion loss results from measurement and simulations for a spring-mass system. Different material models for the foam layer are compared.*

In summary, when selecting an appropriate model for the middle layer in a spring-mass system, its elastic properties play an important role. The poroelastic modeling works better for softer foams, whereas the elastic formulation is more adequate for the prediction with stiffer media. It should be emphasized that in the presented results no attempt has been made to get a better fit by modifying the material parameters. The

employed input parameters have been obtained from common static characterization procedures.

4.3 Three-layered system: Spring-mass system with absorber

The last configuration combines the two systems presented before. For this purpose, an absorbing layer has been placed on the heavy layer of a spring-mass system, forming a three-layered system like the one displayed in Figure 10 (right). The combination of insulation and absorption seems to be an optimal solution, but its industrial application is limited because of space and weight restrictions. Due to the high acoustic efficiency of this system, the radiated power is masked by the background noise already at mid-frequencies and the experimental results can only be reliably evaluated up to 800 Hz. Therefore, the comments regarding the results are limited to this frequency range.

Based on the findings from the results described in the former sections, there is the possibility to model the middle layer of a spring-mass system either as a poroelastic or as an elastic medium, depending on its elastic properties. In turn, the absorber layer may be described with a poroelastic or a porous model depending on its boundary conditions. We have performed the simulations with the corresponding numerical models for the combination of these material formulations for the two foam layers. A selection of the results is shown in Figure 13 as well as the experimental data.

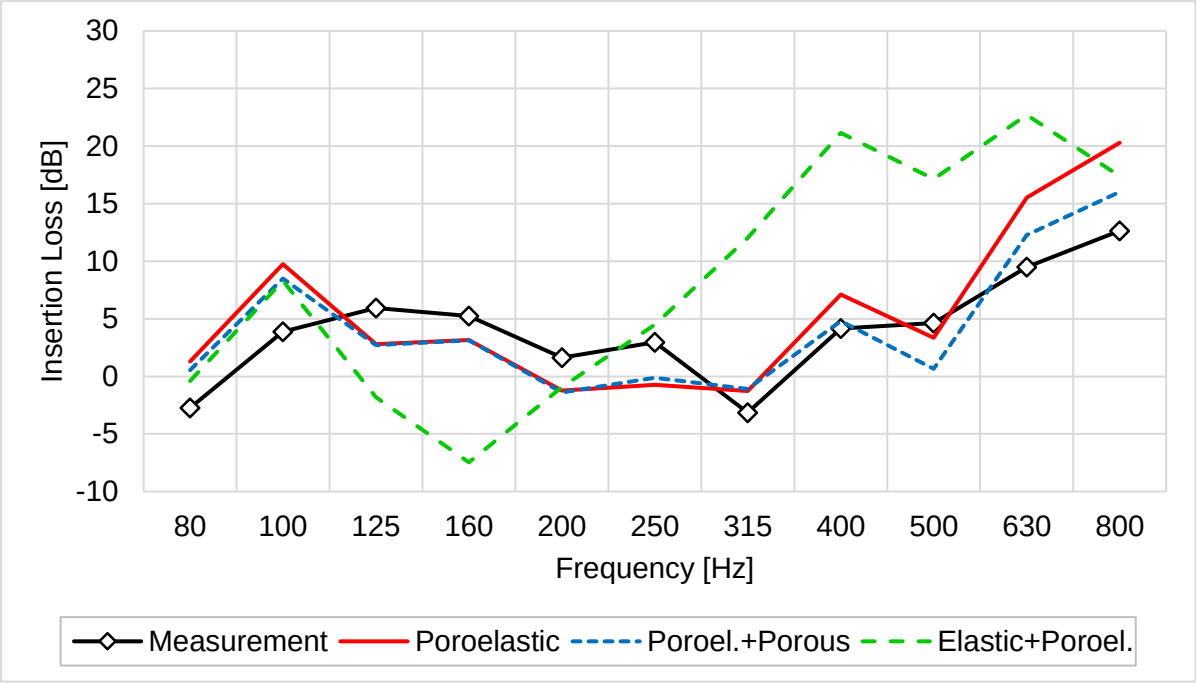

Figure 13. *Insertion loss results from measurement and simulations for a spring-mass system with absorber. Different material models for the two foam layers are compared.*

Firstly, the behavior of the absorber layer is examined by comparing the results under *Poroelastic* (configuration with the two foam layers as poroelastic media) and *Poroel.+Porous* (setup with the spring layer as poroelastic material and the absorber layer as porous medium). We can identify the same trends as for the absorber layer placed on the front of the plastic cover. The poroelastic model predicts a higher IL value because it includes the damping from the solid frame, which increases the total power

dissipated by the complete system. The higher IL level for the poroelastic formulation above 315 Hz points to an interaction between the structural vibration of the heavy layer and the skeleton of the foam when using this material model. Nevertheless, the differences between the results of the two poroelastic models (red and blue curves) are in comparison with to the measurements are too small to give a reliable statement on which model is more suitable.

Secondly, the middle layer of the spring-mass system has been made of a foam with a specific stiffness of E/d = 1.2 kPa/mm, which indicates a relatively soft material. Keeping the absorber layer as a poroelastic medium, we have modeled the spring foam using the elastic formulation (*Elastic+Poroel.* in Figure 13). Analogously to the findings for the soft foam in the former section, the elastic description is not adequate for the representation of the dynamics of the middle foam since the major contribution of the filling air to the total behavior is neglected. Consequently, the simulation results show a softer foam behavior than it actually is. The right choice of the material model for the middle layer is decisive to a correct overall prediction. In contrast, the influence of the chosen material model for the absorber layer is less critical. Besides that, in future experiments either a higher excitation level or another measurement technique is required in order to get a proper validation data set at higher frequencies.

5. Summary and outlook

The need for accurate statements on the acoustic performance of vehicles during the early design phases requires tools that are able to support the development of robust acoustic concepts. In order to predict the airborne noise transmission through complex systems, we have proposed and investigated a hybrid method that combines experimental and numerical approaches.

A proper description of the noise control treatments has been identified as a key factor in the acoustic modeling of the transmission. With help of a simplified front car end model we were able to validate the accuracy of the numerical representation of different concepts for passive treatments based on poroelastic media, such as absorbers and spring-mass systems, provided that an adequate material model is chosen. The application examples presented in the article give an insight into several of the influence factors that should be considered when selecting a material model.

Next steps of the ongoing research include an exhaustive analysis of the input parameters of the poroelastic models, with a special focus on the characterization of the elastic properties as well as their application for simplified material models. As shown in [9], the use of frequency-dependent elastic properties can help to improve the correspondence of the predictions in mid and high frequency ranges. Furthermore, on the global transmission problem, the other subsystems of the noise propagation chain need also to be investigated in detail. The objective is lastly to achieve the integration of the numerical model of the structural component in the complete transmission chain.

Literature

[1] G. Nica (9 June 2016): BMW's Sales Chief Warns about Rapid Change of Auto Industry. Retrieved from http://www.bmwblog.com/2016/06/09/bmw-sales-chief-warns-rapid-change-auto-industry/, Accessed on 07-02-2018.

[2] F. Duvigneau, S. Nitzschke, E. Woschke, U. Gabbert: A holistic approach for the vibration and acoustic analysis of combustion engines including hydrodynamic interactions, Archive of Applied Mechanics 86 (2016) No 11, pp. 1887-1900.

[3] S.F. Wu, L. Kumar Natarajan: Panel acoustic contribution analysis, The Journal of the Acoustical Society of America 133 (2013) No 2, pp. 799-809.

[4] E. Skudrzyk: The foundations of Acoustics – Basic Mathematics and basic Acoustics, Springer Vienna (1971).

[5] M.A. Biot: Theory of propagation of elastic waves in a fluid-saturated porous solid. I. Low frequency range, II. Higher frequency range. The Journal of the acoustical Society of America 28 (1956) No 2, pp.168-191.

[6] J.F. Allard: Propagation of sound in porous media. Modelling sound absorbing materials, Elsevier London, New York (1993).

[7] D. L. Johnson, J. Koplik, R. Dashen: Theory of dynamic permeability and tortuosity in fluid-saturated porous media, Journal of fluid mechanics 176 (1987), pp. 379-402.

[8] Y. Champoux, J.-F. Allard: Dynamic tortuosity and bulk modulus in air saturated porous media, Journal of applied physics 70 (1991) No 4, pp. 1975-1979.

[9] C. Van der Kelen, P. Göransson, B. Pluymers, W. Desmet: On the influence of frequency-dependent elastic properties in vibro-acoustic modelling of porous materials under structural excitation, Journal of Sound and Vibration 333 (2014) No 24, pp. 6560-6571.